

# Polymer Chemistry

Accepted Manuscript



This is an *Accepted Manuscript*, which has been through the Royal Society of Chemistry peer review process and has been accepted for publication.

*Accepted Manuscripts* are published online shortly after acceptance, before technical editing, formatting and proof reading. Using this free service, authors can make their results available to the community, in citable form, before we publish the edited article. We will replace this *Accepted Manuscript* with the edited and formatted *Advance Article* as soon as it is available.

You can find more information about *Accepted Manuscripts* in the [Information for Authors](#).

Please note that technical editing may introduce minor changes to the text and/or graphics, which may alter content. The journal's standard [Terms & Conditions](#) and the [Ethical guidelines](#) still apply. In no event shall the Royal Society of Chemistry be held responsible for any errors or omissions in this *Accepted Manuscript* or any consequences arising from the use of any information it contains.

# Crosslinking of Comb-Shaped Polymer Anion Exchange Membranes Via Thiol-ene Click Chemistry

Liang Zhu†, Tawanda J. Zimudzi†, Nanwen Li†, Jing Pan†, Bencai Lin†, and Michael A. Hickner†\*.

†Department of Materials Science and Engineering, The Pennsylvania State University, University Park, PA 16802, USA

[hickner@matse.psu.edu](mailto:hickner@matse.psu.edu)

**Abstract**

To produce anion conductive and durable polymer electrolytes for alkaline fuel cell applications, a series of cross-linked quaternary ammonium functionalized poly(2,6-dimethyl-1,4-phenylene oxide)s with mass-based ion exchange capacities (IEC) ranging from 1.80 to 2.55 mmol/g were synthesized via thiol-ene click chemistry.  $^1\text{H}$  nuclear magnetic resonance (NMR) spectroscopy and Fourier transform infrared spectroscopy (FTIR) were used to confirm the chemical structure of the samples. From small angle X-ray scattering (SAXS), it was found that the cross-linked membranes developed micro-phase separation between the hydrophilic PPO backbone and the hydrophobic alkyl side chains. The ion conductivity, dimensional stability, and alkaline durability of the cross-linked membranes were evaluated. The hydroxide ion conductivity of the cross-linked samples reached 60 mS/cm in liquid water at room temperature. The chemical stabilities of the membranes were evaluated under severe, accelerated aging conditions and degradation was quantified by measuring ionic conductivity changes during aging. The cross-linked membranes retained their relatively high ion conductivity and good mechanical properties in both 1 M and 4 M NaOH at 80 °C after 500 h. Attenuated total reflection (ATR) spectra were used to study the degradation pathways of the membranes, and it was discovered that  $\beta$ -hydrogen (Hofmann) elimination was likely to be the major pathway for degradation in these membranes.

## Introduction

Polymer electrolyte fuel cells (PEFCs) are efficient energy conversion devices that generate electric power from energy-dense and abundant fuels. Fuel cell technology, in general, is regarded as a promising solution to resolve rising energy demands while reducing the negative environmental impact associated with traditional sources of hydrocarbon energy.<sup>1-3</sup> The polymer electrolyte membrane, which serves as a medium for both ion transport as well as a separator to isolate the cathode from anode during the charging/discharging cycle of a cell, plays a crucial role in the performance of a fuel cell. An ideal polymer electrolyte membrane for fuel cells should demonstrate high ionic conductivity, limited dimensional swelling, low fuel crossover, good thermal and mechanical stability, and facile incorporation into fuel cells.<sup>4,5</sup> Most low-temperature fuel cells are based on proton exchange membranes. Among these acidic membranes, the most common is Nafion<sup>®</sup>, which is a perfluorosulfonic acid-based polymer from DuPont. Nafion<sup>®</sup> is the state-of-the-art proton exchange membrane which has good mechanical and chemical stabilities, and high proton conductivity over a modest relative humidity range.<sup>6-9</sup>

However, PEFCs have some significant drawbacks that hinder widespread commercial application, such as expensive, fluorinated membranes and electrodes that require platinum or precious metal-based catalysts. Alkaline membranes fuel cells (AMFCs) with an anion exchange membrane operating at high pH are currently being studied for their potential to use non-precious metal catalysts in place of platinum.<sup>10,11</sup> The advantages of AMFCs over PEFCs include enhancement of electrode kinetic reactions and more options for cathode catalysts such as non-noble transition metals, improving the performance but reducing the cost of the

devices.<sup>12-17</sup> Extensive efforts have been devoted to enhancing AEMs' performance and stability because these types of low-temperature polymer-based fuel cell materials are currently lagging the development and performance attributes of PEMs. A variety of AEMs, with main backbone structures ranging from poly(arylene ether sulfone)s,<sup>18,19</sup> poly(olefin)s,<sup>20,21</sup> poly(styrene)s,<sup>22-24</sup> poly(phenylene oxide)s,<sup>25,26</sup> poly(phenylene)s,<sup>27</sup> poly(arylene ether)s<sup>18,28-31</sup> to radiated-grafted fluorinated polymers,<sup>32</sup> have been widely investigated, but no consensus currently exists on the most promising pathways forward to high-performance AEMs.

The performance of AMFCs is extremely dependent on certain key requirements of the polymer membrane materials: high ion conductivity ( $> 100$  mS/cm), dimensional durability, and chemical stability. Higher charge carrier densities in AEMs are required because of the lower mobility of hydroxide ions compared to protons. In order to achieve sufficient ion conductivity for AEM applications, high ion-exchange capacities (IEC) are essential for anion exchange membranes. However, increasing the IEC values is most often accompanied by high water uptake, leading to severe dimensional swelling, or even dissolution.<sup>33,34</sup> This trade-off between dimensional stability and ion conductivity creates a need for methods to enhance dimensional stability without compromising ion conductivity.<sup>35</sup> Cross-linking has been reported as an effective method to enhance the dimensional stability of the membrane and to increase the fuel resistance crossover in the preparation of AEMs.<sup>35-50</sup> Several methods have been employed to fabricate cross-linked AEMs. One method is cross-linking via quaternization by diamines, such as *N,N,N',N'*-tetramethylhexanediamine.<sup>50</sup> When halomethylated polymers were quaternized with alkyldiamines, AEMs with enhanced

dimensional integrities, alkaline stabilities, and acceptable hydroxide ion conductivities were achieved.<sup>37,42,43,47,48,50</sup> However, cross-linking through quaternization results in a significant reduction in hydroxide ion conductivity due to the introduction of alkyl chains into the ionic domains and reduced water swelling of the material.<sup>37,42,43,47,48,50</sup> Another approach is to introduce a cationic monomer into a network structure. For example, Zha, *et al.*<sup>51</sup> reported norbornenes with attached ruthenium cations to prepare cross-linked AEMs using ring opening metathesis polymerization (ROMP) and dicyclopentadiene (28.6 mS/cm in hydroxide form, at 30 °C). Robertson, *et al.*<sup>20</sup> developed a new cross-linked AEM using cyclooctene cross-linker with quaternary ammonium groups, which showed good mechanical strength and high ion conductivities (111 mS/cm in hydroxide form, at 50 °C). Previously, PPO and poly(styrene)-based AEMs have been crosslinked using metathesis of pendant side chain double bonds.<sup>40,52</sup> While this strategy was effective at producing highly cross-linked material at room temperature, some residual catalyst could remain in the membranes, which is not ideal for application in fuel cells.<sup>40,52</sup> Additionally, in all of these strategies, the cross-linking of the material occurs as the membrane is cast from solution. Therefore, control of the cross-linking reactions can be difficult and therefore an on-demand cross-linking strategy, such as shown in this work using UV light, may be desirable.

In our previous report, we designed comb-shaped polymers based on poly(2,6-dimethyl-1,4-phenylene oxide) backbones with different lengths of pendant alkyl side chains.<sup>53</sup> These kinds of polymers showed good ion conductivity under alkaline conditions.<sup>53,54</sup> However, due to the increase of ion exchange capacity (IEC), we were unable to obtain membranes with a degree of functionalization (DF) greater than 70 (70 mol % of the

polymer repeat units functionalized) in the pursuit of high-conductivity materials. In order to further enhance ion conductivity, increase dimensional stability, and decrease fuel crossover (such as methanol) in the preparation of new AEMs, we here employ a covalent cross-linking strategy to stabilize comb-shaped AEMs via thiol-ene cross-linking. We introduced side chains with double bonds and used dithiols under UV illumination to accomplish the cross-linking reaction. The advantages of using the thiol-ene click reaction as a strategy for cross-linking are its robustness and efficiency without yielding any harmful byproducts or residue that must be removed from the membrane after the cross-linking reaction has occurred.<sup>55</sup> Also, UV-initiated thiol-ene chemistry was shown to proceed quantitatively with a high degree of specificity within a short time.<sup>55</sup> In the thiol-ene cross-linking of AEMs, it was observed that cross-linked samples exhibited significantly higher dimensional and alkaline stability than that of uncross-linked AEMs. The OH<sup>-</sup> conductivity of X80Y40C6 reached as high as 44 and 200 mS/cm at 20 and 80 °C, while the dimensional stability of the sample was maintained and did not significantly swell as the temperature was raised.

## Experimental

**Materials.** Poly(2,6-dimethyl-1,4-phenylene oxide) was purchased from Sigma-Aldrich and dried under vacuum at room temperature overnight. *N,N*-Dimethylhexylamine, *N,N*-dimethyldecylamine, *N,N*-dimethylhexadecylamine, *N*-bromosuccinimide, 1,8-octanedithiol, and 2,2'-azobis(2-methylpropionitrile) were purchased from Sigma-Aldrich and used as received. The brominated PPO polymers with different degrees of bromination (DB) ranging from 60 to 80% were synthesized according to the reported literature.<sup>56</sup>

**Synthesis of *N,N*-dimethyl-10-undecen-1-amine.**<sup>40</sup> 20 mL 11-Bromo-1-undecene was mixed with 200 mL toluene, and 100 mL THF solution (50 wt % *N,N*-dimethylamine). The resulting mixture was stirred at 60 °C for 2 days. Subsequently, the solution was extracted with satd. NaHCO<sub>3</sub> soln. (3 × 60 mL) and distilled water (3 × 60 mL) sequentially. The resulting organic layer was dried with sodium sulfate, filtered, and concentrated by evaporation of the solvent under vacuum. Finally, the obtained colorless liquid was dried in vacuum at room temperature overnight with a yield of 87 % (mass).

**Polymer synthesis.** Brominated PPO with a DB of 0.6 (1.7 g, 10 mmol) was dissolved in 10 mL of *N*-methyl-pyrrolidone (NMP). Then, *N,N*-dimethyl-10-undecen-1-amine (0.6 g, 3.0 mmol) was added slowly. The mixture was stirred for 48 h at room temperature. Subsequently, *N,N*-dimethylhexylamine (0.46 g, 3.6 mmol) was added, and the mixture was stirred for another 24 h at room temperature. The solution obtained was poured into 200 mL toluene or hexane to precipitate the polymer. The product was filtered and further washed

with hexane and toluene several times. A light yellow powder was obtained and dried under vacuum overnight at room temperature. The resulting product was cross-linkable comb-shaped PPO (X60Y30C6, where the X60 denotes a polymer with 60 mol % DB (total number of PPO repeat units brominated), the Y30 stands for the mol % of cross-linkable alkene groups (out of the total DB of 60 mol %) attached to main chain, and the C6 stands for the length of the alkyl chain) with a yield of 93% (mass) in the bromide form. So, the X60Y30C6 polymer has 30 mol % cross-linking and 30 mol % C6 alkyl amine attachment that remains uncross-linked.

**Fabrication of membranes.** The X60Y30C6 comb-shaped polymer (0.3 g) in the bromide form was dissolved in NMP (5 mL) to form a 5 wt % solution. Subsequently, 1,8-octanedithiol (45 mg, 0.24 mmol) was added to the polymer solution. The mixture was stirred for several minutes at room temperature. Then, 2-benzyl-2-(dimethylamino)-4'-morpholinobutyrophenone (photoinitiator, 30 mg) was added to the mixture. The solution was then cast onto a leveled glass plate, and exposed to UV light (365 nm) for 10 min. The solution was dried at 82 °C under ambient pressure for 24 h followed by vacuum drying for another 24 h at 80 °C to give a thick, transparent, tough film.

**Characterization.**  $^1\text{H}$  nuclear magnetic resonance (NMR) spectra were recorded at 300 MHz on a Bruker AV 300 spectrometer and chemical shifts were listed in parts per million (ppm) downfield from tetramethylsilane (TMS).

Ionic conductivity ( $\sigma$ ) was measured using impedance spectroscopy on a Solartron 1260A impedance/gain phase analyzer with a two-point, in-plane geometry at frequencies ranging from 1 MHz to 100 MHz.<sup>57</sup> The membrane resistance was obtained from the real

value of the impedance where the imaginary response was zero. The  $\sigma$  (mS/cm) of each membrane sample was calculated from  $\sigma = L/RA$ , where  $L$  is the distance between reference electrodes,  $R$  is the resistance of the membrane sample, and  $A$  is the cross-sectional area of the sample. Chloride conductivities were measured by exchanging the bromide form membranes in 1 M sodium chloride at room temperature for 24 h followed by extensively rinsing to remove excess salt with degassed and deionized water. Bicarbonate conductivities were measured by exchanging the chloride form membranes in 1 M sodium bicarbonate for 24 h followed by rinsing to remove excess salt. Hydroxide conductivities were measured by exchanging the bicarbonate form membranes in 1 M potassium hydroxide for 24 h followed by rinsing to remove excess salt. The membranes were subsequently placed into conductivity cells and immersed in deionized water that was degassed and blanketed with flowing argon gas.

The density of the membranes in the hydroxide form was measured by a buoyancy method.<sup>58</sup> Water uptake was measured after drying the membrane in the corresponding counterion form at 60 °C under vacuum for 24 h. The dried membrane was immersed in water and periodically weighed on an analytical balance until a constant mass was obtained, giving the mass-based water uptake. Water uptake was calculated by  $(WU = (m_{\text{hyd}} - m_0)/m_0)$ , where  $m_{\text{hyd}}$  is the hydrated sample mass and  $m_0$  is the dry sample mass. The hydration number ( $\lambda$ ), or the number of water molecules per ionic group, was calculated from:

$$\lambda = \left( \frac{m_{\text{hyd}} - m_0}{m_0} \right) \cdot \left( \frac{1000}{M_{\text{H}_2\text{O}} \cdot \text{IEC}} \right) \quad (1)$$

where  $m_{\text{hyd}}$  is the hydrated membrane mass,  $m_0$  is the mass of the dry membrane,  $M_{\text{H}_2\text{O}}$  is the molecular mass of water ( $18 \text{ g}\cdot\text{mol}^{-1}$ ), and IEC is the ion exchange capacity with units of milliequivalents of ions per gram of polymer. The water volume fraction of the was calculated from:

$$\phi = \left( \frac{\frac{\text{WU}}{\rho_{\text{water}}}}{\frac{\text{WU}}{\rho_{\text{water}}} + \frac{1}{\rho_{\text{membrane}}}} \right) \quad (2)$$

in which WU is the water uptake of membranes,  $\rho_{\text{water}}$  is the density of water ( $1 \text{ g}\cdot\text{cm}^{-3}$ ),  $\rho_{\text{membrane}}$  is the density of dry membranes.

The swelling degree (SW) was characterized by the linear expansion ratio, which was determined using the difference between wet and dry dimensions of a membrane sample (3 cm in length and 1 cm in width). The calculation was based on the following equation:

$$SW(\%) = \frac{X_{\text{wet}} - X_{\text{dry}}}{X_{\text{dry}}} \times 100\% \quad (3)$$

where  $X_{\text{wet}}$  and  $X_{\text{dry}}$  are the lengths of the wet and dry membranes, respectively.

For the cross-linked membranes, the diffusion coefficients of the mobile ions were calculated from a form of the Nernst-Einstein equation:

$$D = \frac{\sigma \cdot R \cdot T}{c \cdot z^2 \cdot F^2} \quad (4)$$

in which,  $\sigma$  is the measured conductivity,  $R$  is the ideal gas constant,  $T$  is the absolute temperature (K),  $c$  is the concentration of ions in moles per  $\text{cm}^3$  calculated by eq. 5,  $z$  is valence charge, and  $F$  is Faraday's constant.<sup>59</sup> The ion concentration,  $c$ , for the membranes was calculated from the volume-based water uptake using:

$$c = 0.001 \cdot \frac{\rho \cdot \text{IEC}}{1 + 0.01 X_{v-\text{H}_2\text{O}}} \quad (5)$$

where  $\rho$  is the polymer density, IEC is the milliequivalents of ion per gram polymer, and  $X_{v-\text{H}_2\text{O}}$  is the volume-based water uptake.<sup>60</sup>

The dilute ion diffusivity can be calculated from the dilute solution mobilities of the mobile ion using the following equation:

$$D_0 = \frac{\mu \cdot k_B \cdot T}{q} \quad (6)$$

in which  $k_B$  is the Boltzmann constant,  $T$  is the absolute temperature (K),  $\mu$  is the dilute solution ion mobility, and  $q$  is the ion charge.<sup>61</sup> The dilute solution mobility of bicarbonate ions, chloride ions, and hydroxide ions are  $46.4 \times 10^{-5} \text{ cm}^2 \cdot \text{V}^{-1} \cdot \text{s}^{-1}$ ,  $76.3 \times 10^{-5} \text{ cm}^2 \cdot \text{V}^{-1} \cdot \text{s}^{-1}$ , and  $197.6 \times 10^{-5} \text{ cm}^2 \cdot \text{V}^{-1} \cdot \text{s}^{-1}$ , respectively.<sup>62,63</sup>

The membranes in the bromide form were immersed in 100 mL of 0.1 M  $\text{NaNO}_3$  standard for 24 h. The solutions were then titrated with a standardized  $\text{AgNO}_3$  solution using  $\text{K}_2\text{CrO}_3$  as an indicator to get the titrated weight-based IEC values ( $\text{IEC}_w$ ).

After cross-linking, the membranes remained insoluble in all common solvents and gel fraction was used to obtain information on the completeness of the cross-linking reaction. The gel fraction of the cross-linked membranes was calculated from the ratio of the weight of the polymer after extraction with NMP at 80 °C for 1 day and the initial weight of the sample.

FTIR spectra were obtained using a Bruker Vertex 70 FTIR spectrometer (Bruker, Billerica, MA) equipped with deuterated triglyceride sulphate (DTGS) detector. ATR

measurements were carried out on membranes on a MVP-Pro ATR accessory (Harrick Scientific Products, Inc. NY) with a diamond ATR crystal at a 45° incidence angle. Transmission spectra were collected on KBr pellets prepared by mixing 2.5 mg of polymer with 60 mg of anhydrous KBr (Sigma-Adrich,). The spectra were signal averaged over 100 scans at 4 cm<sup>-1</sup> resolution with a 5 mm aperture size and a nitrogen purge at ambient temperature. All spectra were processed using Bruker OPUS 6.5 software.

Small-angle X-ray scattering curves of unstained dry counterion form membranes were obtained using a Rigaku instrument equipped with a pinhole camera with an Osmic microfocus Cu K $\alpha$  source and a parallel beam optic. Typical counting times for integration over a multiwire area detector were 1 h with typical membrane thicknesses around 100  $\mu$ m. Measurements were taken under vacuum at ambient temperature on dry samples. Scattering intensities were normalized for background scattering and beam transmission.

## Results and Discussion

***N,N*-dimethyl-10-undecen-1-amine and comb-shaped copolymers synthesis.** The cross-linking reagent *N,N*-dimethyl-10-undecen-1-amine was successfully synthesized from 11-bromo-1-undecene and *N,N*-dimethylamine according to a previous procedure.<sup>40</sup> The chemical structure of this unsaturated dimethyl alkyl amine was confirmed by <sup>1</sup>H NMR spectroscopy and shown in the supporting information (Figure S1). Br-PPO possessing different degrees of bromination (DB) at the benzyl position were synthesized using *N*-bromosuccinimide and 2, 2'-azobis(2-methylpropionitrile) in a refluxing chlorobenzene solution for 3 h according to our previous reports.<sup>40</sup> By altering the usage of

*N*-bromosuccinimide and 2, 2'-azobis(2-methylpropionitrile), Br-PPOs with DB ranging from 60 to 80 were prepared. Then, a series of cross-linkable comb-shaped ionomers ( $X_xY_yC_z$ ) with different side chain length, were achieved by the Menshutkin reaction of the olefinic amine with the bromo group of Br-PPO as shown in Scheme 1 (where the  $x$  stands for DB of PPO;  $y$  refers to the mol % of cross-linkable alkene groups,  $z$  indicates side-chain length). The DB of Br-PPO was set at 60 and 80 to obtain samples with calculated  $IEC_w$ s ranging from 1.80 to 2.55 mmol/g (Table 1). The chemical structures of cross-linkable comb-shaped  $X_{80}Y_yC_6$  cationic copolymers in bromide form were confirmed by  $^1H$  NMR spectroscopy. As is shown in Figure S1, the disappearance of the proton resonance arising from the bromobenzyl moiety as a sharp peak at 4.3 ppm along with the appearance of new peaks at 0.5-1.8 ppm and 3.0 ppm assigned to alkyl chains indicated that the quaternary ammonium groups were formed. The appearance of peaks 5 and 6 in Figure S1 indicated the presence of end alkene groups in the copolymers. Also, the intensity of peaks 5 and 6 increased as the number of cross-linkable alkene groups was increased. The integral ratio of alkene protons, H5 and H6 at 5.8, 5.1 ppm to aromatic peaks at 6.6-7.1 ppm indicated the quaternization reaction was quantitative. Likely, due to the deshielding effect of the quaternary ammonium group, a broad resonance from 4.3 to 4.5 ppm was detected, which could be assigned to the benzylic protons (H11 and H12 in Figure S1).<sup>53</sup>The integral ratio of benzylic protons (H11 and H12 in Figure S1) at 4.3 to 4.5 ppm to the aromatic peaks at 6.6-7.1 ppm indicated the quaternization reaction was quantitative. The  $IEC_w$  of the cross-linkable comb-shaped  $X_{80}Y_yC_6$  membranes calculated from the integrals ratios were consistent with the theoretical values, further suggesting the complete and reliable quaternization of the bromomethyl

groups.

As the 1,8-octanedithiol and photoinitiator showed good solubility in NMP which is also a good solvent for the precursor polymer, all the components of the membrane casting solution were well-distributed to form a homogenous solution. The homogenous solution was cast on a leveled glass plate and exposed to UV light for 10 min before being placed in a convection oven at 80 °C overnight. Ductile, light brown, tough and transparent membranes with a thickness of approximately 70  $\mu\text{m}$  were obtained. The obtained membranes exhibited excellent resistance to polar solvents such as methanol and ethanol indicating high levels of cross-linking. The  $\text{IEC}_w$  values were measured by titration in the range of 1.80 to 2.55 mmol/g, which were in good agreement with values calculated from the  $^1\text{H}$  NMR analysis.

FTIR was used to confirm the reaction of the alkene double bonds with the thiols to form the cross-linked network. As shown in Figure 1, there was a distinct  $\nu$  (C=C) peak at 1639  $\text{cm}^{-1}$  for the uncross-linked X60Y60 membrane, which disappeared after cross-linking along with the  $\nu$  (=C-H) peak at 909  $\text{cm}^{-1}$ .<sup>64</sup> Considering all the evidence and results, a strong covalent cross-linking network was formed by the thiol-ene click cross-linking reaction which was further confirmed by the gel fraction (>80%) in NMP, Table 1. In order to test the reliability and stability of UV-initiated thiol-ene cross-linking method, each experimental condition was repeated three times to prepare three membrane samples, suggesting UV cross-linking was a reliable strategy for cross-linking these copolymers.

**Swelling behavior.** To demonstrate the effect of the degree of cross-linking (DC) on the swelling behavior of the AEM samples, we compared the water uptakes and swelling ratios of

X60Y<sub>y</sub>C6 and X80Y<sub>y</sub>C6 membranes with different degrees of cross-linking (DC). As shown in Figure 2, the thiol-ene cross-linking drastically lowered the water uptake and thus the swelling ratio of the AEMs. Specifically, the cross-linked X80Y40C6 membrane had a water uptake of 144 % and swelling ratio of 25 % at room temperature while the uncross-linked X80Y0C6 sample could be dissolved in water. In addition, the water uptake and swelling ratio of the samples generally decreased with increasing DCs. For example, X60Y15C6 and X60Y60 water uptake were 90 wt % and 43 wt %, and the swelling ratios were 23 % and 10 % at room temperature, respectively. In contrast, uncross-linked X60Y0C6 showed greater water uptake (173 wt %) and swelling ratio (60 wt %) compared to either of the cross-linked samples.

Figure 3 compares the swelling behaviors at elevated temperatures of membranes with different DCs. Although the water uptakes and swelling ratios for all the samples increased with elevated temperatures, increasing the DCs significantly enhanced the dimensional stability of the AEMs. For X60Y30C6 and X80Y40C6, the water uptakes were 67 wt % and 144 wt %, and the swelling ratios were 15 % and 25 % at room temperature, respectively. When the temperature was increased to 80 °C, the water uptake of the samples increased to 93 wt % and 173 wt %, and their swelling ratios went up to 35 % and 48 %, respectively. In comparison, large increases of water uptake and swelling ratio were observed for the uncross-linked X60Y0C6 sample when the temperature was increased from 20 to 80 °C (increases of 157 % for water uptake increment and 130 % for swelling ratio increment). Considering the remarkable agreement between the high solvent resistance and low swelling ratio, a strong covalent cross-linking network was likely formed by the thiol-ene

cross-linking. In addition, it was shown in Figure S2 that longer alkyl side chain restricted the water absorption of AEMs, resulting in lower ion conductivity.<sup>53</sup>

**Ionic conductivity.** High ionic conductivity is one of the most important properties for the application of AEMs in devices. Shown in Figure 4a, the hydroxide conductivity of the cross-linked membranes increased with increasing IEC because of the increase in the water content. When comparing the hydroxide conductivity of the cross-linked and BTMA (benzyltrimethyl ammonium) membranes, the cross-linked membranes demonstrated much higher hydroxide conductivity under the same conditions. For example, the X80Y20C6 membrane with IEC= 2.65 mmol/g showed a conductivity of 60 mS/cm, which was almost three times greater than that of the BTMA40 membrane (23 mS/cm) with an IEC of 2.66 mmol/g. It should also be pointed out that the cross-linked membranes showed much larger hydroxide conductivity than the BTMA<sub>x</sub> membranes under a given hydration number ( $\lambda$ ), Figure 4b.

The hydroxide conductivity of the X60Y<sub>x</sub>C6 and BTMA30 membranes as a function of temperature along with the water uptake of the samples is shown in Figure 5. The hydroxide conductivity steadily increased with increasing temperature and displayed values of 89-200 mS/cm for X80Y<sub>x</sub>C6 membranes at 80 °C, which are greater than the previous reported values for high conductivity AEMs.<sup>18, 21,35-44</sup> For example, Gu, *et al.*<sup>30</sup> reported SCL-TPQPOH with an IEC = 1.23 mmol/g exhibiting hydroxide conductivity of 32.7 mS/cm in water at room temperature. The cross-linked PP-AEMs exhibited synthesized by Zhang, *et al.*<sup>37</sup> hydroxide conductivity of 56.5 mS/cm in deionized water at 80 °C. The cross-linked,

epoxy-based AEMs reported by Zhou, *et al.*<sup>44</sup> exhibited hydroxide conductivity of 14 mS/cm and 78 mS/cm at 30 and 80 °C, respectively. Yang, *et al.*<sup>65</sup> synthesized poly (2, 6-dimethyl-1, 4-phenylene oxide)-*b*-poly (vinylbenzyltrimethylammonium) diblock copolymers based AEMs through growing poly(vinylbenzyl chloride) (PVBC) blocks from a PPO macroinitiator using nitroxide-mediated polymerization. These AEMs exhibited hydroxide conductivity as high as 132 mS/cm in deionized water at 60 °C with IEC = 2.9 mmol/g. The X80Y40C6 sample exhibited the highest OH<sup>-</sup> conductivity (200 mS/cm) at 80 °C, which was nearly six times higher than that of BTMA30 under the same conditions. The X80Y40C6 membranes exhibited the highest hydroxide conductivity above 40 °C due to a trade-off between water uptake, ionic content and conductivity and did not swell greatly like the X80Y20C6 membranes with less crosslinking that showed promising conductivity at lower temperatures. As shown in Figure S3, the HCO<sub>3</sub><sup>-</sup> conductivities of the membranes showed an approximate Arrhenius-type temperature dependence promoted by the thermal activation of water motion.<sup>66</sup> The apparent activation energy estimated from the slopes of the ln( $\sigma$ ) vs 1000/T curves was ~ 12.2 - 22.5 kJ/mol across the measured samples. The apparent activation energies of the tested membranes was comparable to or somewhat lower than those of other reported AEMs (10-23 kJ/mol), indicating that these membranes have a water-facilitated OH<sup>-</sup> conduction mechanism similar to other hydrated AEMs.<sup>66</sup>

After normalizing the samples' hydroxide conductivity on the basis of water volume fraction, the effective hydroxide conductivity in the water channels,  $\sigma'$ , which demonstrates efficiency of the water molecules inside the membranes for transport of hydroxide ions was obtained.<sup>53</sup> All of the cross-linked membranes showed higher  $\sigma'$  than the corresponding

BTMAx samples, as shown in Figure S4. These results indicated that the well-developed micro-phase separation of the cross-linked samples, as discussed in the next section, could efficiently enhance the transport of hydroxide ions.

**Morphological characterization.** More efficient ion transport in anion exchange membranes usually results from better OH<sup>-</sup> transport pathways as the material is hydrated. Generally, for the different AEMs with similar IECs and water uptakes, it is desirable to develop ionic domain aggregation, which ensures ionic channels for good transport. To investigate the microphase separated morphologies of the materials in this study, small-angle x-ray scattering (SAXS) was used to investigate the X60Y60, X60Y30C6, and uncross-linked X60Y60 samples. SAXS profiles, Figure 6, revealed clear scattering peaks for all samples. These results were indicative of nanophase separation between the polar PPO backbone with attached ionic groups and the hydrophobic alkyl side chains. The lack of a second order scattering peak for all the cross-linked membranes demonstrated that no long range ordered structures were formed in these membranes, but only locally correlated arrangement of phase separated domains existed. Generally, the characteristic separation length or interdomain spacing,  $d$ , between the ion-rich domains in ionomers can be calculated by the values of  $q_{\max}$  through the equation  $d = 2\pi/q_{\max}$ . The corresponding interdomain spacing values fall into the range of 3.6 - 4.8 nm, which roughly corresponds to double the length of the extended aliphatic side chains.<sup>53</sup> As shown in Figure 6, the ionic domain peak of the highly cross-linked membrane X60Y60 shifted to lower  $q$  (higher  $d$  value) upon cross-linking likely indicating extension of the ionic domains with the addition of the cross-linking reagent.

In our previous report,<sup>67</sup> we developed a method for analyzing the mobility of ions in PEMs and AEMs via calculating the ion diffusion coefficients ( $D$ ) which included information obtained from conductivity, ion concentration, and water uptake of the polymer membranes. For different ions, we determined the barrier to ion transport via the ratio of the diffusion coefficient to the dilute ion diffusivity ( $D/D_0$ ), where  $D_0$  is the maximum diffusivity of an ion in water.<sup>68</sup> As shown in Figure 7, the  $D/D_0$  ratio increased with increasing hydration for membranes in the hydroxide form, the highest  $D/D_0$  ratio obtained was 0.79 at  $\lambda = 43$  with IEC = 2.41 meq/g for the X80Y20C6 sample. The cross-linked membranes showed relatively higher  $D/D_0$  values than the BTMA membranes at the same  $\lambda$ , suggesting more facile transport of hydroxide in the phase-separated systems as demonstrated by SAXS.

**Membrane Stability.** The long-term stability of AEMs is generally of concern due to known degradation pathways for tetraalkylammonium ions under alkaline conditions, such as  $\beta$ -hydrogen (Hofmann) elimination, direct nucleophilic substitution at the  $\alpha$ -carbon, and benzyl attack.<sup>69-72</sup> The possible degradation mechanism of these membranes is shown in Scheme 2. The products of the different degradation pathways may help to unravel the most prominent degradation mechanisms of the materials. For example, the formation of an alkene accompanies Hofmann elimination while debenzylation results in the appearance of benzyl alcohol. While the signatures of degradation (such as the formation of a tertiary amine during debenzylation and demethylation) maybe convoluted, careful examination of the degradation byproducts will lead to better understanding of the most vulnerable sites for hydroxide attack on these materials and provide a basis for improvement of next-generation membranes.

To evaluate the long-term alkaline stability of the AEMs, X60Y30C6 and uncross-linked X60Y30C6 samples were immersed in argon-saturated 1 M NaOH solution at 80 °C for 500 hours, with replacement of the 1 M NaOH every 3 days during the testing period. Figure 8 illustrates the changes in OH<sup>-</sup> conductivity during stability testing of the samples. During the 500 h test, X60Y30C6 exhibited significantly greater cation stability than that of uncross-linked X60Y30C6. The OH<sup>-</sup> conductivity of X60Y30C6 decreased by 27.0 % and 52.0 %, in 1 M and 4 M NaOH solution, respectively. In contrast, the OH<sup>-</sup> conductivity of uncross-linked X60Y30C6 film decreased by 57.0% and 73.1%, in 1 M and 4 M NaOH solution, respectively. Better stability of the cross-linked AEMs was demonstrated due to the cross-linking of alkyl side chains.<sup>44</sup>

In order to further study the degradation pathways and mechanism, ATR-FTIR spectroscopy was employed to characterize the membranes after being treated in 1 M sodium hydroxide at 80°C. As stated previously, in the AEMs, the major degradation pathways are benzyl attack, direct nucleophilic substitution at the  $\alpha$ -carbon, or  $\beta$ -hydrogen (Hofmann) elimination.<sup>69-72</sup> Analysis of the ATR spectra of membranes after degradation in base provided a method to differentiate between the three mechanisms. Notably, the intensity of the (CH<sub>2</sub>) peak of long alkyl side chains at 2915-2945 and 2840 cm<sup>-1</sup> decreased as the degradation time increased which was shown in Figure 9a, indicating that  $\beta$ -hydrogen (Hofmann) elimination and/or benzyl attack occurred during the testing period.<sup>72</sup> The characteristic benzyl alcohol peaks between 3625 cm<sup>-1</sup> and 3180 cm<sup>-1</sup> were not readily evident in the spectra, indicating that benzyl attack may be a minor pathway in solid membranes, while the  $\beta$ -hydrogen (Hofmann) elimination is a major pathway for degradation.

In addition, the new peaks in Figure 9a, assigned to  $\nu$  (CH) of  $(\text{NCH}_3)_2\text{CH}_2$  appeared at 2975, 2820 and 2770  $\text{cm}^{-1}$ , demonstrate the formation of the  $\text{NC}_3$  group.<sup>75</sup> This observation further confirmed that  $\beta$ -hydrogen (Hofmann) elimination could be the major pathway for degradation in membranes. As shown in Figure 9b, two new peaks assigned to  $\nu$  ( $\text{NC}_3$ ) at 735 and 1035  $\text{cm}^{-1}$  became apparent in the fingerprint region for the degraded membranes.<sup>73</sup> In addition, another new peak assigned to  $\nu$  ( $\text{CH}_2$ ) of  $-\text{CH}_2-\text{NC}_3$  appeared at 1236  $\text{cm}^{-1}$  supporting the formation of the  $\text{NC}_3$  group.<sup>75</sup> The intensity of the peak assigned to  $\nu$  ( $\text{CH}_3$ ) of  $\text{N}^+(\text{CH}_3)_3$  at 1383  $\text{cm}^{-1}$  weakened as the degradation time increased.<sup>76,77</sup> All the degradation information in the ATR-FTIR spectra demonstrated that  $\beta$ -hydrogen (Hofmann) elimination was a major pathway for degradation in these membranes.

## Conclusions

In summary, we have designed and synthesized a new class of cross-linkable, comb-shaped copolymers for stable anion exchange membrane applications. The cross-linked comb-shaped membranes were achieved by thiol-ene click chemistry and the degree of cross-linking was readily controlled by tuning the amount of alkene-containing side chains pendant to the polymer backbone. The obtained cross-linked AEMs displayed a nanoscale phase-separated morphology, which was responsible for the higher ion conductivity of these materials compared to conventional BTMA AEMs. The cross-linking of the membranes enhanced both the chemical and dimensional stability of the membranes. After 500 h immersion in 1 M and 4 M NaOH at 80 °C, the cross-linked membranes maintained significantly higher hydroxide conductivity than those of uncross-linked AEMs. The

ATR-FTIR spectra clearly demonstrated that the major degradation pathway of the quaternary ammonium functionalized poly(2,6-dimethyl-1,4-phenylene oxide)s under alkaline conditions was  $\beta$ -hydrogen (Hofmann) elimination. The combination of the good solubility of the precursor and the highly efficient thiol-ene click chemistry enables this cross-linking strategy as a promising technology for preparing attractive AEM materials for fuel cells applications.

### AUTHOR INFORMATION

Corresponding Author

hickner@matse.psu.edu

### ACKNOWLEDGMENTS

This work was funded by the Advanced Research Projects Agency – Energy (ARPA-E), U.S. Department of Energy, under award number: DE-AR0000121 and the United States-Israel Binational Science Foundation (BSF) through Energy Project No. 2011521.

### Reference

- 1 A. J. Appleby, and F. R. Foulkes, *Fuel Cell Handbook*, Van Nostrand Reinhold: New York, 1989.
- 2 L. Carratte, K. A. Friedlich, and U. Stimming, *Fuel Cells*, 2001, **1**, 5-39.
- 3 B. C. H. Steele, and A. Heinzl, *Nature*, 2001, **414**, 345-352.
- 4 G. Merle, M. Wessling, and K. Nijmeijer, *J. Membr. Sci.*, 2011, **377**, 1-35.
- 5 J. J. Fontanella, M. G. McLin, M. C. Wintersgill, J. P. Calame, and S. G. Greenbaum, *Solid State Ionics*, 1993, **66**, 1-4.
- 6 C. H. Lee, H. B. Park, Y. M. Lee, and R. D. Lee, *Ind. Eng. Chem. Res.*, 2005, **44**,

7617-7626.

7 R. F. Silva, M. De Francesco, and A. Pozio, *J. Power Sources*, 2004, **134**, 18-26.

8 A. Filipi, M. Boccia, and H. A. Gasteiger, *ECS Trans.*, 2008, **16**, 1835-1845.

9 J. R. Vorcoe, and R. C. T. Slade, *Fuel Cells*, 2005, **2**, 187-200.

10 T. Xu, *J. Membr. Sci.*, 2005, **263**, 1-29.

11 M. A. Hickner, *Mater. Today*, 2010, **13**, 34-41.

12 T. S. Olson, S. Pylypenko, P. Atanassov, K. Asazawa, H. Yamada, and H. Tanaka, *J. Phys. Chem. C*, 2010, **114**, 5049-5059.

13 J. Sanabria-Chinchilla, K. Asazawa, T. Sakamoto, K. Yamada, T. Tanaka, and P. Strasser, *J. Am. Chem. Soc.*, 2011, **133**, 5425-5431.

14 J. Pan, C. Chen, L. Zhuang, and J. Lu, *Acc. Chem. Res.*, 2012, **45**, 471-483.

15 Y. Wang, J. Qiao, R. Baker, and Zhang, *J. Chem. Soc. Rev.*, 2013, **42**, 5768-5787.

16 J. R. Varcoe, R. C. T. Slade, G. L. Wright, and Y. L. Chen, *J. Phys. Chem. B*, 2006, **110**, 21041-21049.

17 X. Wu, and K. Scott, *J. Power Sources*, 2012, **206**, 14-19.

18 J. Yan, and M. A. Hickner, *Macromolecules*, 2010, **43**, 2349-2356.

19 N. Li, Q. Zhang, C. Wang, Y. M. Lee, and M. D. Guiver, *Macromolecules*, 2012, **45**, 2411-2419.

20 N. J. Robertson, H. A. Kostalik IV, T. J. Clark, P. F. Mutolo, H. D. Abruña, and G. W. Coates, *J. Am. Chem. Soc.*, 2010, **132**, 3400-3404.

21 K. J. Noonan, K. M. Hugar, H. A. Kostalik IV, E. B. Lobkovsky, H. D. Abruña, and G. W. Coates, *J. Am. Chem. Soc.*, 2012, **134**, 18161-18164.

- 22 T. H. Tsai, A. M. Maes, M. A. Vandiver, C. Versek, S. Seifert, M. Tuominen, M. W. Liberatore, A. M. Herring and E. B. Coughlin, *J. Polym. Sci., Part B: Polym. Phys.*, 2012, **51**, 1751-1760.
- 23 Q. H. Zeng, Q. L. Liu, I. Broadwell, A. M. Zhu, Y. Xiong, X. P. Tu, *J. Membr. Sci.*, 2010, **349**, 237-243.
- 24 Y. Luo, J. Guo, C. Wang, and D. Chu, *J. Power Sources*, 2010, **195**, 3765-3771.
- 25 L. Wu, G. Zhou, X. Liu, Z. H. Zhang, C. Li, and T. Xu, *J. Membr. Sci.*, 2011, **371**, 155-162.
- 26 A. D. Mohanty, Y.-B. Lee, L. Zhu, M. A. Hickner, and C. Bae, *Macromolecules*, 2014, **47**, 1973-1980.
- 27 M. R. Hibbs, C. H. Fujimoto, and C. J. Cornelius, *Macromolecules*, 2009, **42**, 8316-8321.
- 28 M. R. Hibbs, M. A. Hickner, T. M. Alam, S. K. McIntyre, C. Y. Fujimoto, and C. Cornelius, *J. Chem. Mater.*, 2008, **20**, 2566-2573.
- 28 J. Zhou, M. Unlu, J. A. Vega, and P. A. Kohl, *J. Power Sources*, 2009, **190**, 285-292.
- 29 J. Wang, S. Li, and S. Zhang, *Macromolecules*, 2010, **43**, 3890-3896.
- 30 S. Gu, R. Cai, and Y. Yan, *Chem. Commun.*, 2011, **47**, 2856-2858.
- 31 Z. Zhao, J. Wang, S. Li, and S. Zhang, *J. Power Sources*, 2011, **196**, 4445-4450.
- 32 J. R. Varcoe, R. C. T. Slade, E. L. H. Yee, S. D. Poynton, D. J. Driscoll, and D. C. Apperley, *Chem. Mater.*, 2007, **19**, 2686.
- 33 J. R. Varcoe, P. Atanassov, D. R. Dekel, A. M. Herring, M. A. Hickner, P. A. Kohl, A. R. Kucernak, W. E. Mustain, K. Nijmeijer, K. Scott, T. Xu, and L. Zhuang, *Energy Environ. Sci.*, 2014, **7**, 3135.

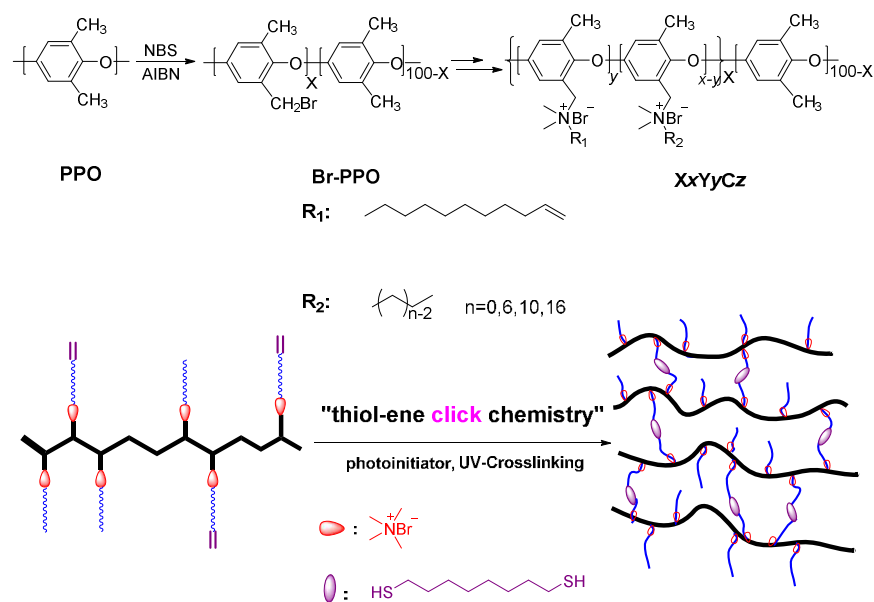
- 34 J. Pan, S. Lu, Y. Li, A. Huang, L. Zhuang, and J. Lu, *Adv. Funct. Mater.*, 2010, **20**, 312-319.
- 35 T. H. Tsai, S. P. Ertem, A. M. Maes, S. Seifert, A. M. Herring, and E. B. Coughlin, *Macromolecules*, 2015, **48**, 655-662.
- 36 J. Pan, L. Zhu, J. Han, and M. A. Hickner, *Chem. Mater.*, 2015, **27**, 6689-6698.
- 37 M. Zhang, J. Liu, Y. Wang, L. An, M. D. Guiver, and N. Li, *J. Mater. Chem. A*, 2015, **3**, 12284-12296
- 38 Y. Z. Zhuo, A. N. Lai, Q. G. Zhang, A. M. Zhu, M. L. Ye, and Q. L. Liu, *J. Membr. Sci.*, 2015, **491**, 138-148.
- 39 B. Lin, F. Chu, Y. Ren, B. Jia, N. Yuan, H. Shang, T. Feng, Y. Zhu, and J. Ding, *J. Power Sources*, 2014, **266**, 186-192.
- 40 N. Li, L. Wang, and M. A. Hickner, *Chem. Commun.*, 2014, **50**, 4092-4095.
- 41 B. Lin, H. Dong, Y. Li, Z. Si, F. Gu, and F. Yan, *Chem. Mater.*, 2013, **25**, 1858-1867.
- 42 X. Lin, Y. Liu, S. D. Poynton, L. Ong, A. J. R. Varcoe, L. Wu, Y. Li, X. Liang, Q. Li, and T. Xu, *J. Power Sources*, 2013, **233**, 259-268.
- 43 Y. Zhao, H. Yu, D. Yang, J. Li, Z. Shao, and B. Yi, *J. Power Sources*, 2013, **221**, 247-251.
- 44 J. F. Zhou, M. Unlu, I. Anestis-Richard, and P. A. Kohl, *J. Membr. Sci.*, 2010, **350**, 286-292.
- 45 C. C. Yang, S. J. Chiu, W. C. Chien, and S. S. Chiu, *J. Power Sources*, 2010, **195**, 2212-2219.
- 46 B. Lin, L. Qiu, J. Lu, and F. Yan, *Chem. Mater.*, 2010, **22**, 6718-6725.
- 47 Y. Xiong, J. Fang, Q. H. Zeng, and Q. L. Liu, *J. Membr. Sci.*, 2008, **311**, 319-325.

- 48 D. Stoica, L. Ogier, L. Akrou, F. Alloin, and J. F. Fauvarque, *Electrochim. Acta*, 2007, **53**, 1596-1603.
- 49 Y. H. Wu, C. M. Wu, T. W. Xu, F. Yu and Y. X. Fu, *J. Membr. Sc.*, 2008, **321**, 299-308.
- 50 J. S. Park, S. H. Park, S. D. Yim, Y. G. Yoon, W. Y. Lee, and C. S. Kim, *J. Power Sources*, 2008, **178**, 620-626.
- 51 Y. Zha, M. L. Disabb-Miller, Z. D. Johnson, M. A. Hickner, and G. N. Tew, *J. Am. Chem. Soc.*, 2012, **134**, 4493-4496.
- 52 L. Wang and M. A. Hickner, *Polym. Chem.*, 2014, **5**, 2928-2935.
- 53 N. W. Li, Y. J. Leng, M. A. Hickner, and C. Y. Wang, *J. Am. Chem. Soc.*, 2013, **135**, 10124-10133.
- 54 A. Amel, L. Zhu, M. Hickner, and Y. Ein-Eli, *J. Electrochem. Soc.*, 2014, **161**, F615-F621.
- 55 K. L. Killops, L. M. Campos, and C. J. Hawker, *J. Am. Chem. Soc.*, 2008, **130**, 5062-5064.
- 56 N. Li, T. Yan, Z. Li, T. Thurn-Albrecht, and W. H. Binder, *Energy Environ. Sci.*, 2012, **5**, 7888-7892.
- 57 C. H. Fujimoto, M. A. Hickner, C. J. Cornelius, and D. A. Loy, *Macromolecules*, 2005, **38**, 5010-5016.
- 58 W. Xie, H. Ju, Geise, M. G. B. D. Freeman, J. I. Mardel, A. J. Hill, and J. E. McGrath, *Macromolecules*, 2011, **44**, 4428-4438.
- 59 H. J. Walls, P. S. Fedkiw, T. A. Zawodzinski, and S. A. Khan, *J. Electrochem. Soc.*, 2003, **150**, E165- E174.
- 60 Y. Kim, B. Einsla, M. Sankir, W. Harrison, and B. Pivovar, *Polymer*, 2006, **47**, 4026.
- 61 M. Muthukumar, *Advances in Chemical Physics*, Rice, S. A., Ed.; 2005; Vol. 131, p. 45.

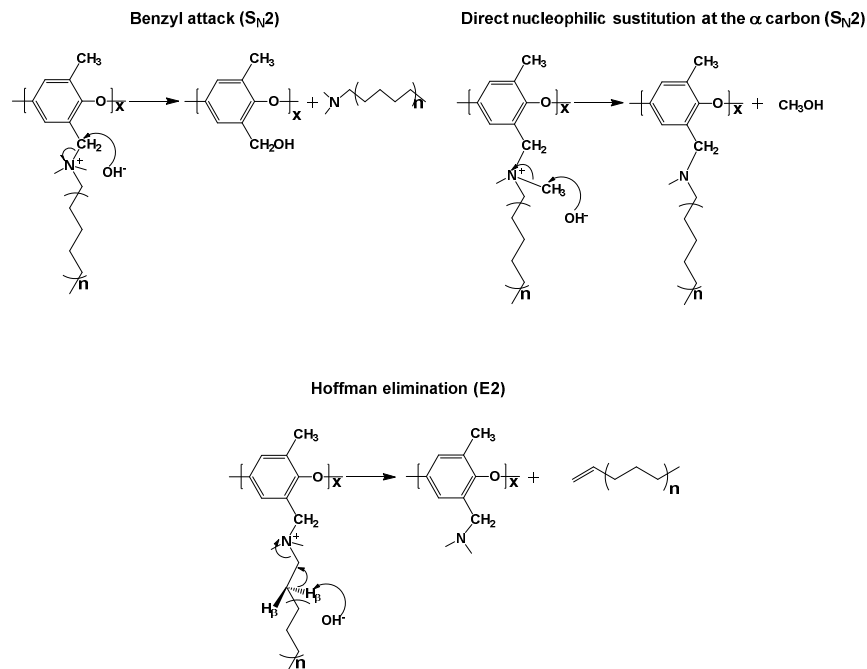
- 62 D. Voet, and J. G. Voet, *Biochemistry*, Fourth.; John Wiley & Sons, 2011; p. 45.
- 63 P. Vanysek, *CRC Handbook of Chemistry and Physics*, Lide, D. R., Ed.; CRC Press: Boca Raton, 2002.
- 64 M. Slavons, M. Laurent, J. Devaux, and V. Carlier, *Polymer*, 2005, **46**, 8062-8067.
- 65 Y. Yang, and D. M. Knauss, *Macromolecules*, 2015, **48**, 4471-4480.
- 66 D. Chen, and M. A. Hickner, *Macromolecules*, 2013, **46**, 9270-9278.
- 67 M. L. Disabb-Miller, Y. Zha, A. J. DeCarlo, M. Pawar, G. N. Tew, and M. A. Hickner, *Macromolecules*, 2013, **46**, 9279-9287.
- 68 M. L. Disabb-Miller, Z. D. Johnson, and M. A. Hickner, *Macromolecules*, 2013, **46**, 949-956.
- 69 J. R. Varcoe, and R. C. T. Slade, *Fuel Cells*, 2005, **2**, 187-200.
- 70 S. A.; Nuñez, and M. A. Hickner, *ACS Macro Lett.*, 2013, **2**, 49-52.
- 71 S. Chempath, B. R. Einsla, L. R. Pratt, C. S. Macomber, J. M. Boncella, J. A. Rau, and B. S. Pivovar, *J. Phys. Chem. C*, 2008, **112**, 3179-3182.
- 72 B. R. Einsla, S. Chempath, L. R. Pratt, J. M. Boncella, J. Rau, C. Macomber, and B. S. Pivovar, *Electrochem. Soc. Trans.*, 2007, **11**, 1173-1180.
- 73 C. S. Macomber, J. M. Boncella, B. S. Pivovar, and J. A. Rau, *J. Therm. Anal. Calorim.*, 2008, **93**, 225-229.
- 74 W. Zhou, N. Yao, G. Yao, C. Deng, X. Zhang, and P. Yang, *Chem. Commun.*, 2008, **43**, 5577-5579.
- 75 J. N. Gayles, *Spectrochim. Acta*, 1967, **23**, 1521-1531.
- 76 K. O. Christe, W. W. Wilson, R. D. Wilson, R. Bau, and J. A. Feng, *J. Am. Chem. Soc.*,

1990, **112**, 7619-7625.

77 E. A. V. Ebsworth, and N. Sheppard, *Spectrochim. Acta*, 1959, **13**, 261-270.



Scheme 1. Synthesis of cross-linked comb-shaped AEMs,  $X_xY_yC_z$ , with one alkyl side chain using thiol-ene click chemistry.



Scheme 2. Possible degradation pathways of the quaternary ammonium cations in the membranes.

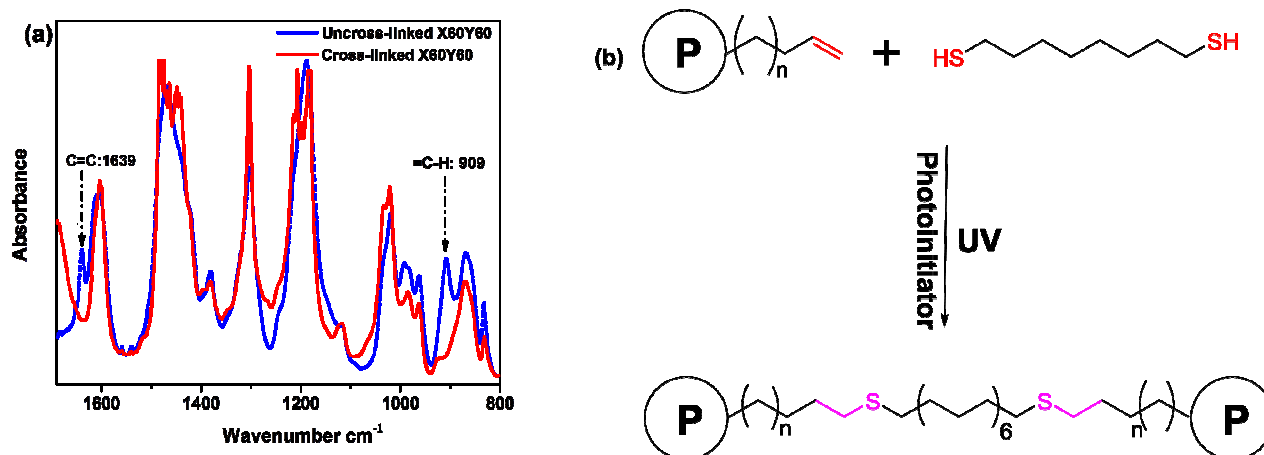


Figure 1. FTIR spectra of uncross-linked and cross-linked membranes (a) and schematic plot of cross-linked reaction (b).

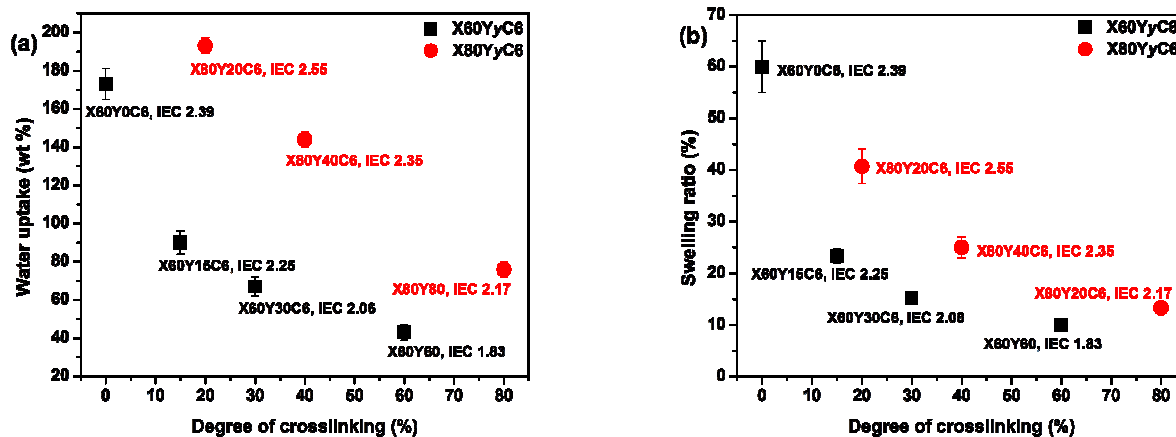


Figure 2. Liquid water uptake (a) and swelling ratio (b) of membranes in OH<sup>-</sup> form as a function of degree of cross-linking at room temperature.

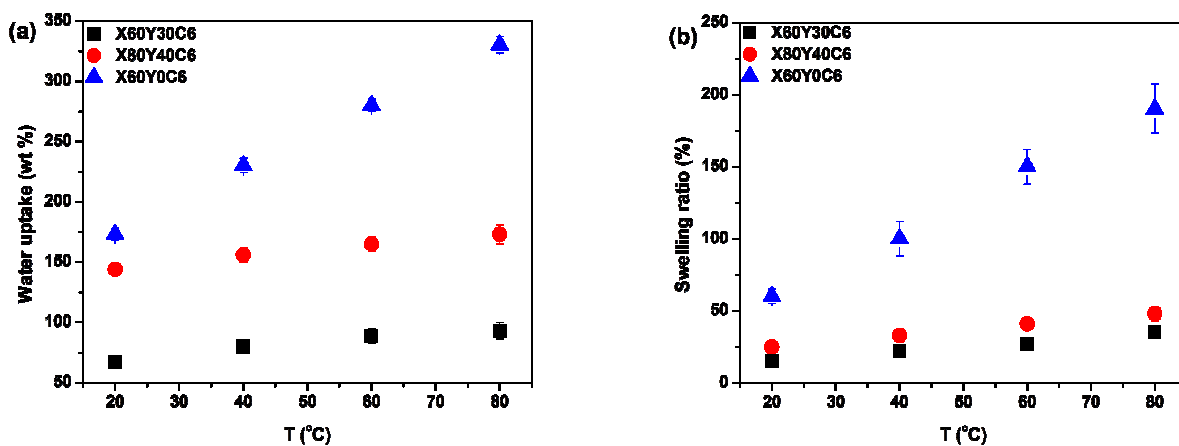


Figure 3. Liquid water uptake (a) and swelling ratio (b) of membranes in OH<sup>-</sup> form as a function of temperature.

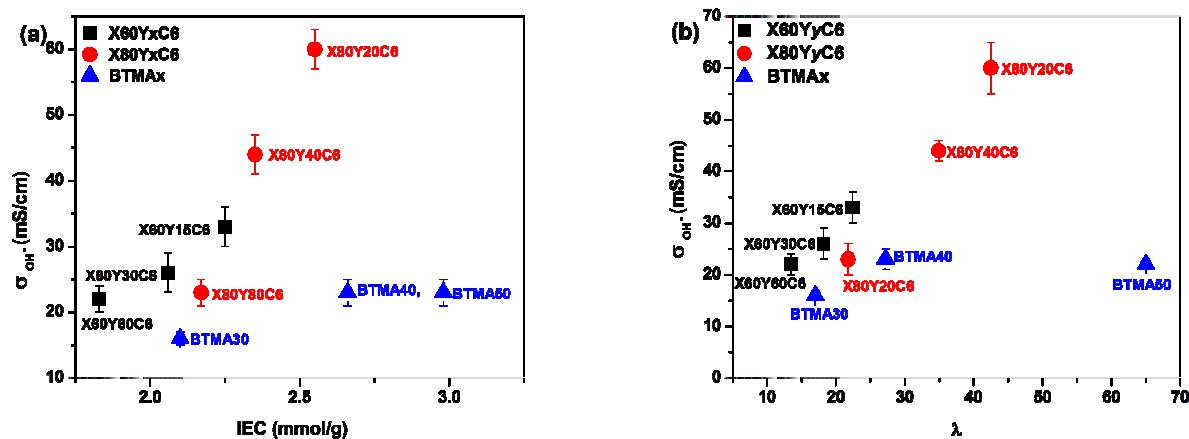


Figure 4. Hydroxide conductivity of membranes as a function of (a) IEC (ion exchange capacity) and (b) hydration number  $\lambda$  (moles of water per mole of quaternary ammonium group) in water at room temperature. Conductivities were measured with samples exposed to liquid water.

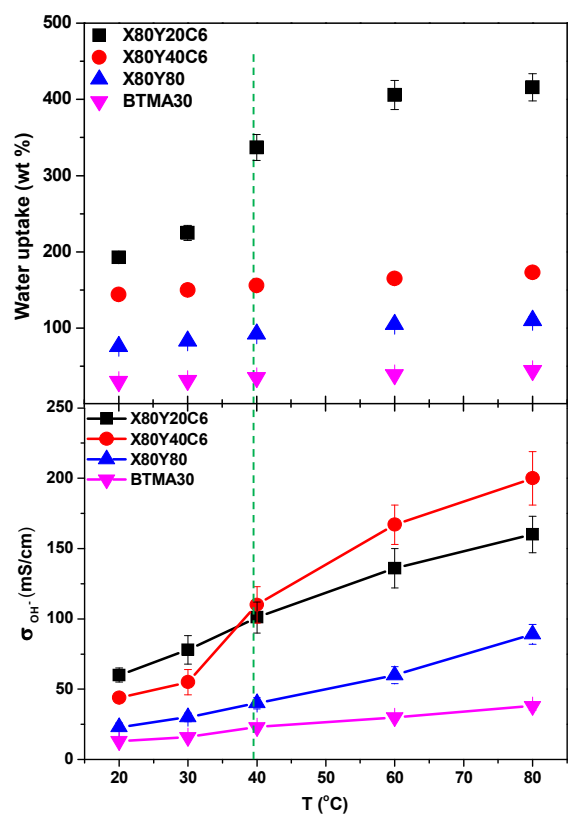


Figure 5. Hydroxide conductivity of X80YxC6 and BTMA30 membranes as a function of temperature. Conductivities were measured with samples exposed to liquid water.

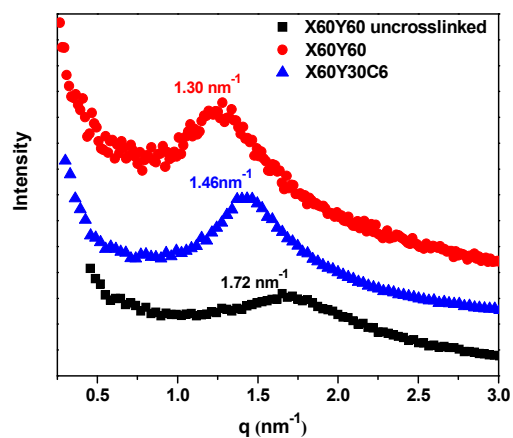


Figure 6. SAXS profiles of dry polymer membranes in the bromide form.

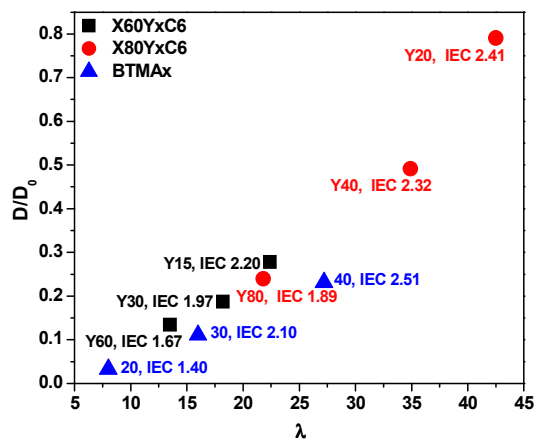


Figure 7. Ratio of the diffusion coefficient,  $D$ , to the dilute solution diffusivity,  $D_0$ , as a function of hydration number for membranes in the hydroxide form.

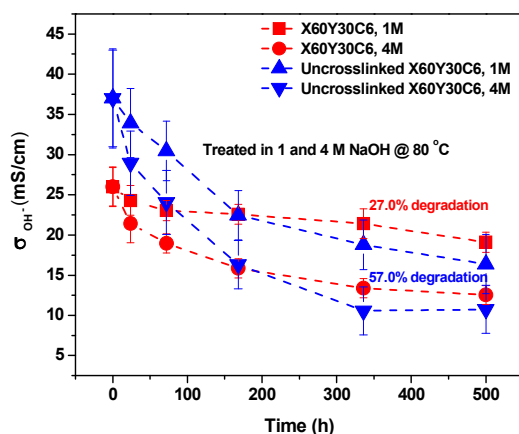


Figure 8. Chemical stability of the quaternary ammonium cation of X60Y30C6 and uncross-linked X60Y30C6 in 1 M and 4 M NaOH solution at 80 °C, and OH<sup>-</sup> conductivity as a function of duration time measured at 20 °C.

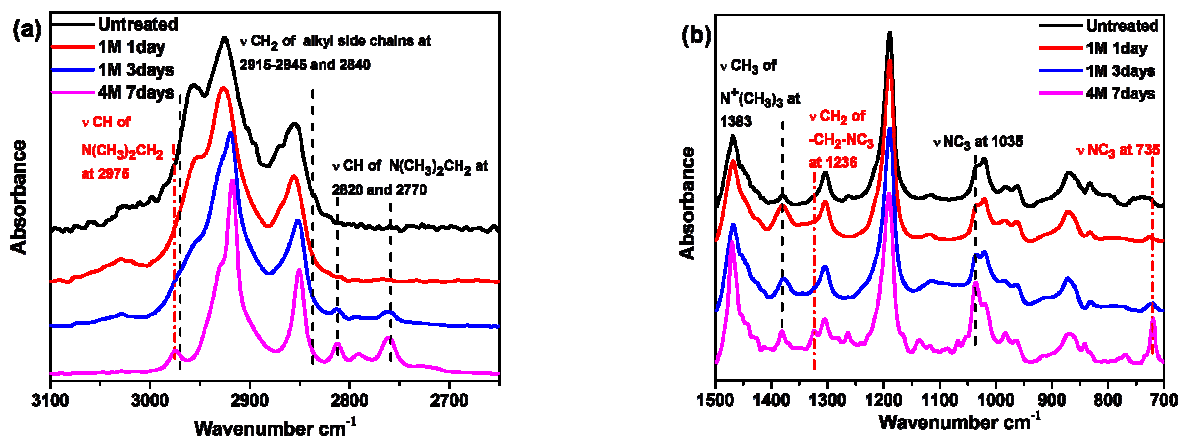


Figure 9. ATR spectra of treated X60Y15C6 membrane (a) ATR spectra of functional group region (b) fingerprint region.

Table 1. Ion exchange capacity, water uptake, swelling and conducting behaviors of cross-linked AEMs.

sample	IEC (mmol/g) <sup>a</sup>	IEC (mmol/g) <sup>b</sup>	WU (%) (OH) <sup>d</sup>	WU (%) (HCO <sub>3</sub> ) <sup>c</sup>	WU (%) (Cl) <sup>c</sup>	$\sigma$ (OH) <sup>c</sup>	$\sigma$ (HCO <sub>3</sub> ) <sup>c</sup>	$\sigma$ (Cl) <sup>c</sup>	$\lambda$ (OH)	Swelling ratio (%) <sup>c</sup>	Gel fraction (%)
<b>X60Y15C6</b>	2.51	2.25	90 ± 6	47 ± 3	31 ± 2	33 ± 3	5.3 ± 0.3	8.9 ± 0.4	22.4	23.3 ± 1.4	83
<b>X60Y30C6</b>	2.38	2.06	67 ± 5	41 ± 2	22 ± 2	26 ± 3	4.2 ± 0.2	6.7 ± 0.5	18.2	15.2 ± 0.9	87
<b>X60Y60</b>	2.10	1.83	43 ± 4	34 ± 2	15 ± 3	22 ± 2	3.2 ± 0.2	4.2 ± 0.2	13.5	10.6 ± 0.7	89
<b>X60Y30C10</b>	2.26	2.03	58 ± 5	39 ± 3	21 ± 2	22 ± 2	4.1 ± 0.2	5.4 ± 0.3	16.6	14.5 ± 0.7	89
<b>X60Y30C16</b>	2.07	1.80	46 ± 2	33 ± 2	18 ± 2	17 ± 1	3.3 ± 0.2	4.9 ± 0.2	14.2	13.2 ± 0.8	90
<b>X80Y20C6</b>	2.94	2.55	193 ± 4	56 ± 3	43 ± 4	60 ± 5	12.2 ± 1.1	14.9 ± 1.2	42.5	40.7 ± 3.3	87
<b>X80Y40C6</b>	2.63	2.35	144 ± 4	43 ± 3	30 ± 3	44 ± 2	8.4 ± 0.7	10.9 ± 0.5	34.9	25.0 ± 2.0	92
<b>X80Y80</b>	2.39	2.17	76 ± 3	24 ± 3	13 ± 2	23 ± 3	3.8 ± 0.3	5.8 ± 0.3	21.8	13.3 ± 0.8	95
<b>X80Y40C10</b>	2.52	2.20	49 ± 3	31 ± 3	20 ± 1	21 ± 3	5.1 ± 0.3	7.6 ± 0.4	12.7	15.4 ± 1.1	95
<b>X80Y40C16</b>	2.41	2.08	26 ± 1	20 ± 2	12 ± 1	18 ± 2	3.4 ± 0.2	4.8 ± 0.3	7.3	9.5 ± 0.6	96

<sup>a</sup>Calculated from the polymer composition and the degree of bromination. <sup>b</sup>Titrated values. <sup>c</sup>The membranes in OH<sup>-</sup> form were used for measurements of the swelling ratio at room temperature in water.

## TOC

